MHSA: A Multi-scale Hypergraph Network for Mild Cognitive Impairment Detection via Synchronous and Attentive Fusion

1st Manman Yuan
School of Computer Science
Inner Mongolia University
Hohhot 010000, China
yuanman@imu.edu.cn

2nd Weiming Jia
School of Computer Science
Inner Mongolia University
Hohhot 010000, China
csjwm@mail.imu.edu.cn

3rd Xiong Luo*
School of Computer and
Communication Engineering
University of Science and Technology Beijing
Beijing 100083, China
xluo@ustb.edu.cn

4th Jiazhen Ye*
School of Computer Science
Inner Mongolia University
Hohhot 010000, China
jiazhenye@mail.imu.edu.cn

5th Peican Zhu
School of Artificial Intelligence,
Optics and Electronics
Northwestern Polytechnical University
Xi'an 710072, Shaanxi, China
ericcan@nwpu.edu.cn

6th Junlin Li
Department of Imaging Medicine
Inner Mongolia Autonomous
Region People's Hospital
Hohhot, 010017, China
grefor@163.com

***Abstract*—The precise detection of mild cognitive impairment (MCI) is of significant importance in preventing the deterioration of patients in a timely manner. Although hypergraphs have enhanced performance by learning and analyzing brain networks, they often only depend on vector distances between features at a single scale to infer interactions. In this paper, we deal with a more arduous challenge, hypergraph modelling with synchronization between brain regions, and design a novel framework, i.e., A Multi-scale Hypergraph Network for MCI Detection via Synchronous and Attentive Fusion (MHSA), to tackle this challenge. Specifically, our approach employs the Phase-Locking Value (PLV) to calculate the phase synchronization relationship in the spectrum domain of regions of interest (ROIs) and designs a multi-scale feature fusion mechanism to integrate dynamic connectivity features of functional magnetic resonance imaging (fMRI) from both the temporal and spectrum domains. To evaluate and optimize the direct contribution of each ROI to phase synchronization in the temporal domain, we structure the PLV coefficients dynamically adjust strategy, and the dynamic hypergraph is modelled based on a comprehensive temporal-spectrum fusion matrix. Experiments on the real-world dataset indicate the effectiveness of our strategy. The code is available at https://github.com/Jia-Weiming/MHSA.**

***Index Terms*—Mild cognitive impairment, Hypergraphs, Brain networks, Phase-Locking Value, Multi-scale feature fusion**

I. Introduction

Mild cognitive impairment (MCI) detection through hypergraphs represents a fundamental challenge in the intersection of biology and artificial intelligence. Early studies, such as Ding et al. [1], Shao et al. [2], and Ji et al. [3] employ a hypergraph learning strategy for the detection of MCI. In recent years, with the evolution of deep learning methodologies [4], researchers have utilized data features of various models to construct multimodal hypergraphs [5]–[7], significantly refreshing the state-of-the-art records.

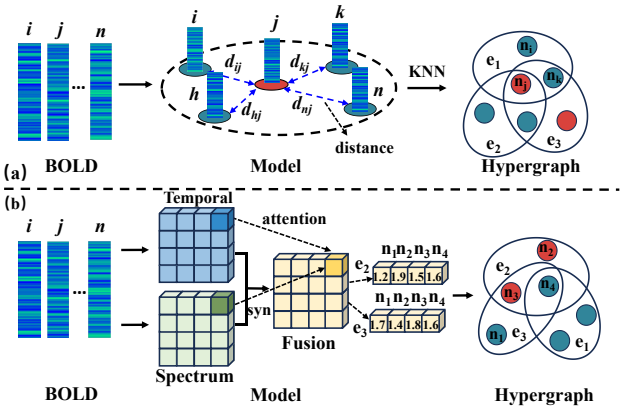

Fig. 1. Modeling approaches for high-order brain networks. (a) Existing methods rely on vector distances. It lacks biological explainability. (b) In contrast, our proposed approach, MHSA, is dependent on incorporating features from both the temporal and spectrum domains of BOLD signals. This significantly improves the dynamic properties of brain network construction.

However, current studies [4], [8], [9] on hypergraph construction rely on vector distances to deduce similarities between brain regions, as illustrated in Fig. 1, encompassing details such as spatial proximity and functional connectivity. Indeed, acquiring such signal scale features

*Corresponding author

is intensely challenging in reflecting dynamic functional connectivity changes and some temporal impossible in describing the complex synchronized interactions of biological signals between corresponding ROIs [10], [11].

To our knowledge, no existing studies consider the MCI detection problem with synchronous information. In practice, functional magnetic resonance imaging (fMRI) sequences can reflect continuous dynamic changes of ROIs in the temporal domain when brains perform specific tasks [12], [13], and different ROIs demonstrate phase dependencies in the spectrum domain [14], as evidenced by their well-characterized phase synchronization attributes. MCI detection with hypergraphs poses two main challenges.

First, vector distances are overly dependent on inferred interactions in geometric space, which will lose the dynamic connectivity patterns and complex interactions between regions. Second, it is difficult to align and optimize the connection effectiveness in the process of multi-scale feature fusion. Intuitively, to handle the above issues, we should 1) fully exploit the phase synchronization information of signals; and 2) adaptively refine connection strengths employing phase synchronous indicators.

In this paper, we propose a Multi-scale Hypergraph Network with Synchronous and Attentive Fusion for MCI Detection. First, the PLV is introduced to quantify the phase synchronization of fMRI signals in the spectrum domain. Second, we employ an attention algorithm to evaluate and optimize the direct contribution of each ROI to phase synchronization in the temporal domain and dynamically adjust the PLV coefficients, yielding a comprehensive temporal-spectrum fusion matrix. Finally, an adaptive hypergraph is modeled based on the above matrix, and MCI detection is realized by learning its graph representations.

Overall, our contribution is summarized as follows:

- We are the first to consider the synchronization between ROIs during the process of MCI detection and propose a new method to address this issue.
- We formulate a multi-scale hypergraph construction method to integrate the dynamic connectivity of fMRI via synchronous and attentive fusion strategy.
- We demonstrate the effectiveness and superiority of the proposed method in the ADNI dataset, compared to baseline approaches.

II. RELATED WORK

The construction of brain networks from neuroimaging data for brain disease detection is a prominent research topic. Conventional methods typically rely on direct relationships between node pairs and utilize Graph Convolutional Networks (GCNs) to extract disease-related features. For instance, Ma et al. [15] construct multi-view brain networks for Alzheimer's Disease (AD) diagnosis by leveraging the temporal series similarity of ROIs, which are then processed by a GCN to extract node embeddings. Zhao et al. [16] propose a self-learning spatial-temporal GCN for enhanced preclinical AD diagnosis. Meanwhile, Ma et al. [17] develop a multi-graph cross-attention network to improve MCI classification performance. However, these methods establish only pairwise connections between brain regions and fail to capture higher-order interactions and associations, resulting in an incomplete representation of the brain network's structure and function.

Recently, employing hypergraphs to model brain networks and capture intricate higher-order interactions has gained considerable attention. Liu et al. [18] utilize a spatio-temporal weighted hypergraph convolutional network to capture high-order brain activity patterns, thereby enhancing MCI classification. The dwHGCN model [19] adaptively refines hyperedge weights during training to improve the learning of brain functional connectivity features. Meanwhile, Li et al. [20] have developed a hypergraph attention network that leverages attentive feature aggregation for MCI classification. Despite these advancements, these methods still rely on direct vector distances between brain signals, which inadequately represent their true functional connections.

Additionally, some approaches analyze interactions between brain regions in the spectrum domain to capture more accurate topological relationships within brain networks. For instance, Wang et al. [21] dynamically capture spatial topological structures by analyzing multichannel EEG in the frequency domain using the PLV. Similarly, Wang et al. [22] investigate emotional states by constructing brain networks in the spectrum domain with PLV, thereby assessing functional connectivity differences across various emotions. Unfortunately, the connections within brain networks are both complex and diverse, neither focusing on a single signal domain nor just establishing higher-order relationships can fully simulate brain activity. Thus, our method captures both spectrum and temporal relationships in brain signals, constructing a higher-order network that more comprehensively represents the complex information transmission and interactions within the brain.

III. METHODOLOGY

In this paper, the multi-scale hypergraph is constructed via a synchronous and attentive fusion strategy for MCI detection. The overall architecture of the proposed model is illustrated in Fig. 2. Subsequently, the implementation of MHSA will be described.

A. Synchronization analysis model

PLV is a crucial method for calculating the synchrony characteristic of electrophysiological signals at specific frequencies, and the regional synchrony is proportional to the correlation between the signals. We calculate the PLV value between the pairwise ROI temporal signals x_i and x_j to evaluate the degree of phase synchronization, as below:

$$PLV_{ij} = \frac{1}{T}\left|\sum_{l=1}^{T} e^{\mathcal{I}(\triangle\phi_{ij}(t_l))}\right|, \tag{1}$$

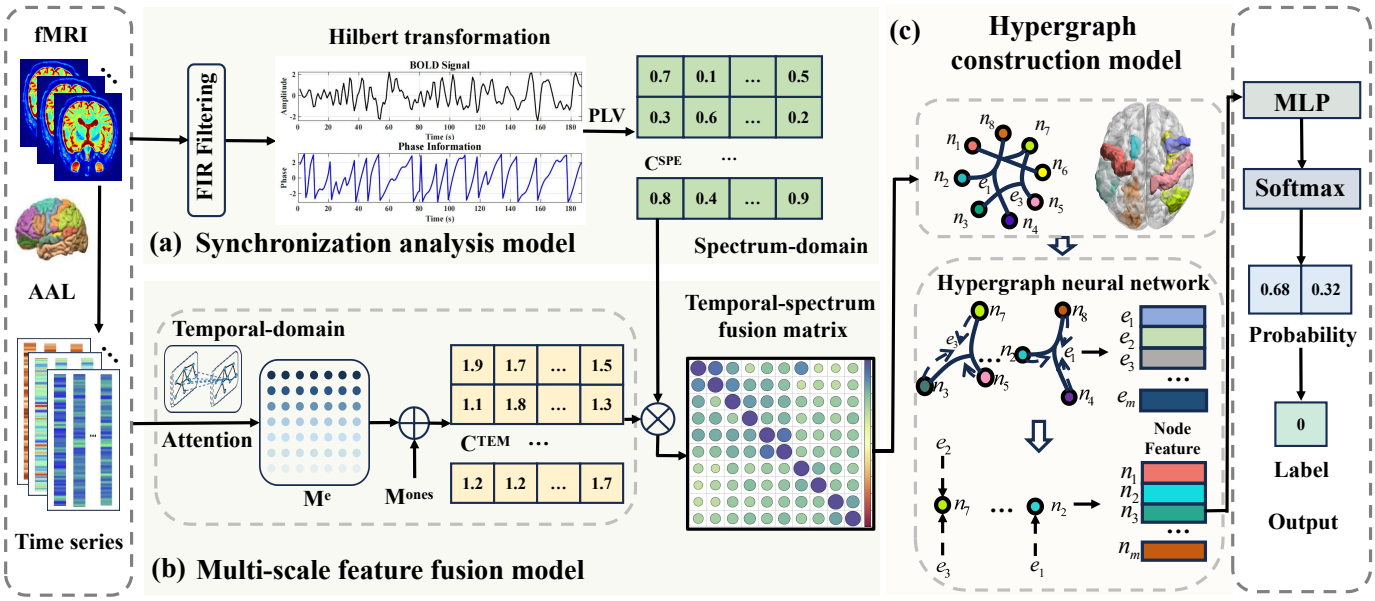

Fig. 2. Illustration of MHSA. (a) We conduct a Hilbert transform on the BOLD signals to extract phase information, which is then utilized for phase synchronization analysis in the spectrum domain, culminating in the derivation of C^{SPE}. (b) We employ an attention algorithm to assess the temporal-domain importance of ROIs, followed by an optimization using the smoothing matrix M^{ones} to ensure an equitable integration of information across all brain regions, and finally synthesizing this with C^{SPE} into a comprehensive temporal-spectrum fusion matrix. (c) We construct a hypergraph based on the fusion matrix and advance to graph feature representation learning through a hypergraph neural network.

where $\triangle\phi_{ij}(t_l) = (\phi_i(t_l) - \phi_j(t_l))$ stands for the instantaneous phase difference between temporal signal, which $\phi_i(t_l)$ and $\phi_j(t_l)$ are computed from $x_i(t_l)$ and $x_j(t_l)$ respectively, using the Hilbert transform [23] to obtain the phase values. The $l \in \{1, 2, \ldots, T\}$ represents a temporal segments within T, and $\mathcal{I}$ represents the imaginary unit. Afterward, we leverage the synchronous correlation among ROIs to form second-order spectrum-matrix $C^{SPE} \in \mathbb{R}^{N\times N}$, defined as follows:

$$C_{ij}^{SPE} = PLV_{ij}. \tag{2}$$

B. Multi-scale feature fusion model

Considering the real change of practical bioelectrical signal transmission during the process of contributing brain networks, we focus on a multi-scale feature fusion mechanism to integrate dynamic connectivity features of fMRI from both the temporal domain and spectrum domain. Specifically, C^{SPE} provides the synchronization relationship of ROIs in the spectrum domain. Then, the attention mechanism [24] is employed to calculate the weight coefficient among the ROIs signals x_i and x_j as the connection strength in the temporal domain:

$$e_{ij} = \frac{\exp(\text{LeakyReLU}(a^\intercal([W_e x_i \parallel W_e x_j])))}{\sum_{k\in\mathcal{N}_i}\exp(\text{LeakyReLU}(a^\intercal([W_e x_i \parallel W_e x_k])))}, \tag{3}$$

where $a^\intercal \in \mathbb{R}^{2T\times 1}$ and W_e are a parameterized vector and a learnable weight matrix, respectively. $\parallel$ is the concatenation operation. And e_{ij} computes the degree of association between ROIs signals x_i and x_j in the temporal domain, and $\mathcal{N}_i$ represents the set of nodes directly related to the signal x_i if C_{ij}^{SPE} is greater than a preset threshold τ. Furthermore, an attention matrix $M^e \in \mathbb{R}^{N\times N}$ is defined with $M_{ij}^e = e_{ij}$ to represent the correlation between all ROIs on the temporal domain, and the minimization optimization function is utilized to obtain the best combination of learnable parameters:

$$\mathcal{L}_{opt} = \sum_{i,j=1}^{N} \|x_i - x_j\|_2^2 M_{ij}^e + \lambda \|M^e\|_{\mathrm{F}}^2, \tag{4}$$

where $\lambda \geq 0$ is a regularization parameter. To prevent attention from overly concentrating on specific pairs of ROIs, we define an all-ones matrix $M^{ones} \in \mathbb{R}^{N\times N}$ to smooth the attention matrix M^e, enabling the model to evenly consider information from all brain regions.

$$C^{TEM} = M^e + M^{ones}, \tag{5}$$

where C^{TEM} is a smoothed temporal-domain matrix.

Finally, from the view of multi-scale, C^{TEM} and C^{SPE} are combined through a Hadamard product to unveil the synchronicity and dynamic changes between ROIs:

$$C^{TS} = C^{TEM} \odot C^{SPE}. \tag{6}$$

C. Hypergraph construction model

In this section, the temporal-spectrum matrix C^{TS} is utilized to form a hypergraph for feature representation. Initially, a hypergraph is represented by $\mathcal{G}(\mathcal{V}, \mathcal{E}, \mathcal{W})$, where $\mathcal{V} = \{v_1, v_2, \ldots, v_n\}$ denotes the node set and $\mathcal{E} = \{e_1, e_2, \ldots, e_m\}$ represents the hyperedge set, which each e connects multiple nodes and is weighted by a diagonal

matrix of $\mathcal{W}$. Afterwards, the hypergraph $\mathcal{G}$ is expressed through a $|\mathcal{V}| \times |\mathcal{E}|$ incidence matrix H, defined as follows:

$$H(v,e) = \begin{cases} 1 & if\ v \in e, \\ 0 & if\ v \notin e. \end{cases} \tag{7}$$

Then, the hyperedge construction is according to C^{TS}. For each ROI i, select K in C^{TS} the associated regions with the highest connection value, defined as set top_K$_i$. Based on this, the incidence matrix H is redefined as:

$$H(i,j) = \begin{cases} 1 & \text{if } j \in \text{top\_K}_i, \\ 0 & \text{otherwise.} \end{cases} \tag{8}$$

For the incidence matrix H, its vertex degree matrix is defined as $D_v = \text{diag}(\{d(v_i)\}_{i=1}^n)$ with $d(v) = \sum_{e \in \mathcal{E}} w(e) H(v,e)$, and the hyperedge degree matrix represents as $D_e = \text{diag}(\{\delta(e_i)\}_{i=1}^m)$, where $\delta(e) = \sum_{v \in \mathcal{V}} H(v,e)$. Finally, hypergraph neural networks (HGNNs) [25] are utilized to capture higher-order relationships between ROIs for feature representation, which the ℓ-th convolution layer can be represented as:

$$X^{\ell+1} = \sigma(D_{\text{v}}^{-1/2} H W D_{\text{e}}^{-1/2} H^T D_{\text{v}}^{-1/2} X^{(\ell)} \Theta^{(\ell)}), \tag{9}$$

where $X^{(\ell)}$ denotes the convolution output features of the ℓ-th layer, $\Theta^{(\ell)}$ as a filter is applied to extract node features in hypergraphs, and $W = \text{diag}(\{w(e_i)\}_{i=1}^m)$ denotes a learnable hyperedge weight matrix.

D. Readout and Classification

After feature extraction by hypergraph neural networks, the output Z is used for graph-level reading and disease classification. Then, a multilayer perceptron is trained to derive the prediction:

$$\hat{y} = MLP(Z). \tag{10}$$

For $\mathcal{T}$ samples of subjects, the predicted label $\hat{y}_t$ and true label y_t are taken as the input of a cross-entropy function to estimate the prediction loss:

$$\mathcal{L} = -\frac{1}{\mathcal{T}} \sum_{\mathcal{T}} [y_t \cdot \log(\hat{y}_t) + (1 - y_t) \cdot \log(1 - \hat{y}_t)]. \tag{11}$$

IV. EXPERIMENTS AND RESULTS

A. Experiments on task-related ADNI dataset

In this study, brain imaging data was collected from the Alzheimer's Disease Neuroimaging Initiative (ADNI) dataset[1]. ADNI facilitates the sharing of global data on AD in its early stages. The initiative attempts to explore interventions, prevention, and treatment strategies for MCI and AD by using various biomarkers. Our study selected 179 subjects, including 51 patients with mild cognitive impairment (MCI), 64 patients with early MCI (EMCI), 36 patients with late MCI (LMCI), and 28 age-matched normal controls (NC). The details of demographics and clinical characteristics are presented in Table I.

[1]http://www.adni-info.org/

TABLE I
DETAILS OF THE SUBJECTS

Group	Number	Gender		Age
		Male	Female	
MCI	51	33	18	74 ± 18
EMCI	64	39	25	77 ± 15
LMCI	36	18	18	72 ± 11
NC	28	16	12	77 ± 13

The Data Processing Assistant for Resting-State fMRI (DPARSF) package was used in this study to preprocess the raw functional images and extract the ROI fMRI temporal series. This multi-step process is as follows: first, slice timing correction is performed by removing the first 10 temporal points. Then, motion correction is conducted, and subjects with head movement exceeding 2.5 mm or 2.5 degrees are excluded. Next, Statistical Parametric Mapping (SPM) is employed to realize co-registration with T1-weighted structural images and perform subsequent segmentation into gray matter, white matter, and cerebrospinal fluid; then, normalization is applied to the Montreal Neurological Institute (MNI) space using DARTEL. Subsequently, functional images are smoothed with a 4mm full width at half-maximum (FWHM) Gaussian kernel to reduce registration variability. Finally, bandpass filtering is performed on the functional temporal series between 0.01 and 0.1 Hz.

B. Baselines

The MHSA method is compared with existing baselines, including well-estimated graph methods and specifically designed brain network analysis models.

- **SVM** [26]: A classical supervised machine learning algorithm achieves data classification by optimizing the feature space's hyperplane margin.
- **GCN** [27]: A classical graph learning algorithm. Its core idea is to simplify the polynomial convolution to a first-order form and realize information aggregation in a one-hop neighborhood.
- **GAT** [24]: A classical spatial graph convolution algorithm. Its core idea is to determine the node importance of the first-order neighborhood by using the self-attention mechanism for localized convolution.
- **GCNII** [28]: An effective extended model of GCN. The model is improved using the initial residual and identity mapping technology so that the convolutional layer can stack multiple layers. It performs well in heterogeneous and homogeneous graph processing.
- **GCNH** [29]: A spatially localized convolution inspired by spectrum methods. Its core idea is to sparsify a generalized form of graph diffusion to effectively alleviate the issues of noisy edges and arbitrary definitions encountered in real graphs.

TABLE II
CLASSIFICATION RESULTS BY 5-FOLD CROSS-VALIDATION WITH COMPETING METHODS.

Method	NC vs. EMCI (%)				NC vs. MCI (%)				NC vs. LMCI (%)			
	Accuracy	Sensitivity	Precision	F1	Accuracy	Sensitivity	Precision	F1	Accuracy	Sensitivity	Precision	F1
SVM	72.87 ± 7.48	79.62 ± 8.03	81.00 ± 6.20	80.14 ± 6.09	64.50 ± 5.34	59.09 ± 7.84	82.50 ± 10.00	68.06 ± 5.12	70.18 ± 10.21	76.0 ± 14.97	69.54 ± 16.72	70.73 ± 9.78
GCN	71.63 ± 8.65	60.00 ± 17.89	73.67 ± 6.00	65.33 ± 13.43	68.50 ± 7.52	76.73 ± 15.58	76.92 ± 8.35	75.42 ± 6.63	71.64 ± 8.65	60.0 ± 17.89	73.67 ± 6.0	65.33 ± 13.43
GAT	82.57 ± 5.42	$\mathbf{96.92 \pm 3.77}$	82.09 ± 6.50	88.65 ± 3.23	63.08 ± 8.56	84.00 ± 20.59	67.64 ± 5.62	73.53 ± 1.24	62.55 ± 16.56	72.00 ± 3.92	48.26 ± 13.46	56.96 ± 15.08
GCNII	78.30 ± 5.63	89.23 ± 6.15	82.07 ± 6.90	85.16 ± 3.63	82.25 ± 2.67	$\mathbf{100.0 \pm 0.0}$	78.53 ± 2.48	87.95 ± 1.53	71.64 ± 8.65	64.00 ± 14.97	75.76 ± 14.39	67.67 ± 10.20
GCNH	66.43 ± 10.08	67.31 ± 14.70	82.56 ± 11.43	72.81 ± 10.02	73.50 ± 13.21	86.91 ± 17.94	75.31 ± 5.49	80.20 ± 11.23	66.36 ± 8.41	64.00 ± 14.97	70.00 ± 17.89	63.74 ± 8.26
CAGNN	72.87 ± 9.12	89.10 ± 14.24	76.68 ± 6.21	81.58 ± 7.39	64.67 ± 4.33	74.73 ± 22.92	78.06 ± 14.52	71.75 ± 7.83	56.73 ± 10.31	72.00 ± 3.49	64.02 ± 19.97	57.05 ± 14.60
SiGAT	68.65 ± 14.11	93.90 ± 8.43	70.67 ± 13.07	79.86 ± 9.15	68.42 ± 5.25	92.72 ± 14.55	69.88 ± 5.76	78.63 ± 5.29	63.64 ± 17.81	48.33 ± 20.96	44.50 ± 19.00	44.72 ± 18.79
HGNN	76.02 ± 8.38	85.64 ± 9.94	81.02 ± 6.95	82.99 ± 7.04	78.58 ± 11.47	88.36 ± 11.43	81.26 ± 9.74	84.11 ± 8.54	72.18 ± 15.87	72.00 ± 20.40	72.09 ± 21.07	70.52 ± 17.16
MHSA	$\mathbf{86.96 \pm 5.39}$	$\mathbf{96.92 \pm 3.77}$	$\mathbf{86.61 \pm 5.93}$	$\mathbf{91.29 \pm 3.29}$	$\mathbf{86.08 \pm 9.98}$	98.0 ± 4.0	$\mathbf{84.13 \pm 10.42}$	$\mathbf{90.26 \pm 6.92}$	$\mathbf{83.45 \pm 15.56}$	$\mathbf{84.0 \pm 14.97}$	$\mathbf{84.26 \pm 20.40}$	$\mathbf{83.13 \pm 15.28}$

TABLE III
CLASSIFICATION RESULTS BY 5-FOLD CROSS-VALIDATION WITH COMPETING METHODS.

Method	NC vs. ALL TYPES of MCI (%)			
	Accuracy	Sensitivity	Precision	F1
SVM	77.65 ± 3.05	81.51 ± 5.58	91.28 ± 2.48	85.94 ± 2.33
GCN	84.37 ± 1.27	$\mathbf{100.0 \pm 0.0}$	84.37 ± 1.27	91.51 ± 0.74
GAT	84.36 ± 1.27	$\mathbf{100.0 \pm 0.0}$	84.37 ± 1.27	91.51 ± 0.74
GCNII	89.98 ± 5.96	97.42 ± 5.16	91.43 ± 3.71	94.24 ± 3.49
GCNH	85.46 ± 5.14	91.33 ± 6.18	91.53 ± 3.12	91.28 ± 3.25
CAGNN	87.14 ± 3.79	97.33 ± 5.33	89.04 ± 5.04	92.75 ± 2.10
SiGAT	86.10 ± 6.06	99.29 ± 1.43	86.18 ± 5.86	92.18 ± 3.54
HGNN	87.70 ± 3.81	$\mathbf{100.0 \pm 0.0}$	87.39 ± 3.62	93.23 ± 2.03
MHSA	$\mathbf{92.21 \pm 3.66}$	$\mathbf{100.0 \pm 0.0}$	$\mathbf{91.65 \pm 3.68}$	$\mathbf{95.60 \pm 2.02}$

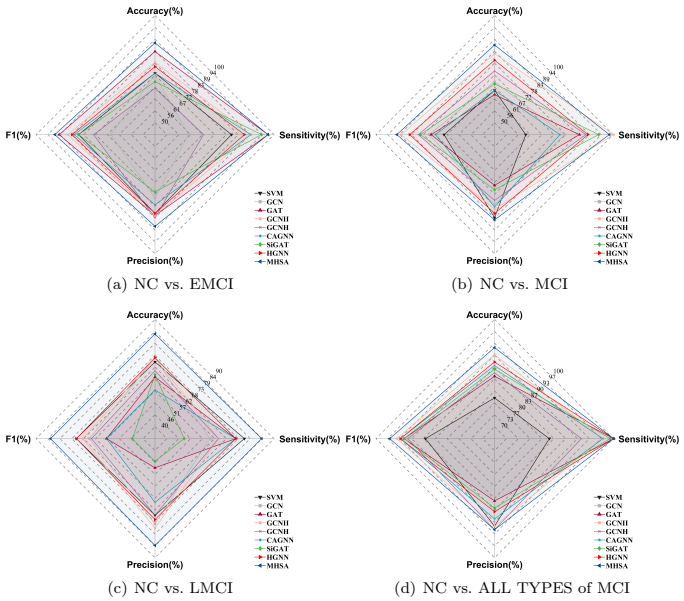

(a) NC vs. EMCI (b) NC vs. MCI (c) NC vs. LMCI (d) NC vs. ALL TYPES of MCI

Fig. 3. Performance comparison among competing methods in tasks of MCI detection.

- **CAGNN** [30]: An algorithm specifically designed for heterogeneous networks. It decouples node features into discriminative features for downstream tasks, aggregates features for graph convolutional layers and fuses the two features for classification through a shared mixer module.
- **SiGAT** [31]: The SiGAT offers a new graph learning method for directed signed networks, utilizing social network theories and attention mechanisms to produce effective node embeddings.
- **HGNN** [25]: HGNN extends the convolution operation to the domain of hypergraph learning. It implements spectrum convolution using hypergraph Laplacian, which is then efficiently approximated by truncated Chebyshev polynomials.

To demonstrate the advantage of our MHSA model in classifying MCI, four evaluation metrics were used: accuracy, sensitivity, precision, and F1-score. The optimal parameter combinations for all methods were identified using five-fold cross-validation and grid parameter optimization, and fair comparisons were conducted within a unified PyTorch environment equipped with an NVIDIA GeForce A800 GPU.

C. Main disease prediction results

In this section, the performance of MHSA in different MCI classification tasks is introduced in detail. Firstly, to validate the capacity of MHSA to distinguish between various subtypes of MCI, as shown in Table II, the ADNI dataset was divided into three specific classification tasks: NC vs. MCI, NC vs. LMCI, and NC vs. EMCI. The experimental results suggest that MHSA outperformed others in almost all evaluation metrics for these tasks. Meanwhile, to evaluate the efficacy of MHSA in the broader MCI classification task, as shown in Table III, MCI, LMCI, and EMCI were consolidated into a single disease category for comparison with NC. The experimental outcomes indicate that MHSA is more competitive on this task and demonstrates an overall leading effect. It outperforms the sub-optimal by 2.23% in accuracy and achieves a perfect score of 100% in sensitivity, showcasing its exceptional recognition capability. In terms of precision, it exceeds the second-best model by 0.12%. Additionally, in the F1 score, an indicator of the model's overall effectiveness, we have seen a 1.36% improvement over the second-ranked model. Overall, the experimental results in the two tables, along with the illustrative visualization in Fig. 3, fully demonstrate the advantage of MHSA in the task of MCI detection.

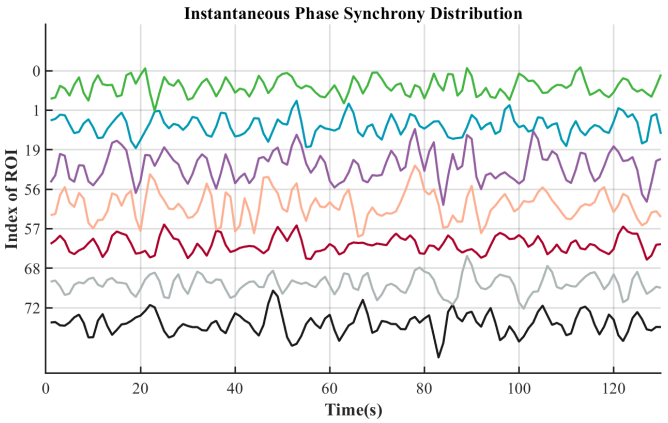

Fig. 4. Phase synchronization analysis focusing on ROIs interconnected by the same hyperedge within complex network structures.

D. Hyperedge analysis in brain networks

The properties of hyperedge connections were analyzed in depth, with a focus particularly on the synchronization among multiple ROIs connected by the same hyperedge. The results, shown in Fig. 4, reveal a significant level of synchronization. This synchronization highlights the critical role of hyperedges in connecting different brain regions and demonstrates the collaborative dynamics in these regions during cognitive processes. The analysis of such synchronicity is the key to unveiling the intricate mechanisms underlying information transfer and neural computation in brain networks.

Then, our analysis of brain networks in various MCI states focuses on the properties of the hyperedge. Fig. 5 demonstrates a significant difference in the number of vertices connected on the same hyperedge at different stages of MCI. The results suggest that to achieve the best detection effect of MCI at different stages, the number of vertices connected by one hyperedge is different. This difference may be related to the neurobiological mechanisms of cognitive decline, providing a potential avenue for further investigation into MCI.

Moreover, we quantified the connectivity of individual brain regions by determining the number of hyperedges

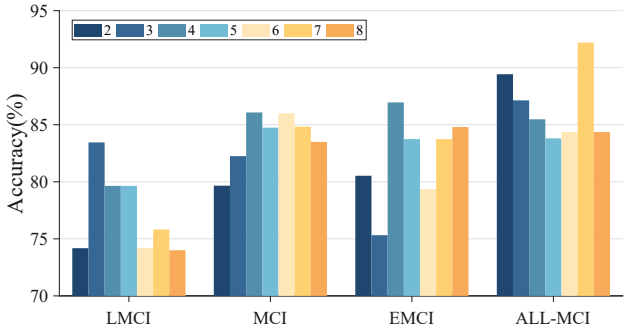

Fig. 5. The number of vertices connected on edges at different stages of MCI corresponds to the effect of classification.

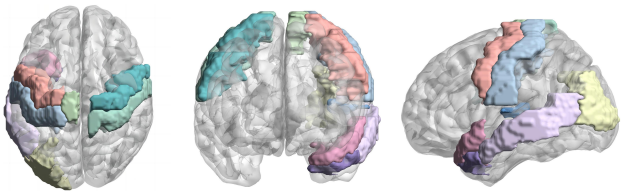

Fig. 6. Top 10 brain regions with the highest connectivity in the MCI pathological network are depicted from various perspectives.

associated with each region and concentrated on the 10 regions exhibiting the highest connectivity, respectively regions PreCG.R, PreCG.L, TPOsup.L, CAU.L, PCL.L, MTG.L, PoCG.L, MOG.L, TPOmid.L and PoCG.R, as depicted in Fig. 6. We propose that these regions are pivotal within the pathological network of MCI, not only occupying central positions within the brain network but also demonstrating strong associations between functional connectivity, metabolic activity, and structural integrity with cognitive function. Further examination of these regions equips medical professionals with a robust tool for more precisely predicting MCI progression, thereby providing a strong scientific foundation for early diagnosis and personalized treatment development.

E. Ablation analysis

A variety of extensive experiments were undertaken to confirm the significance of two pivotal elements of MHSA: PLV and the attention mechanism. PLV provides a synchronous analysis tool that can adeptly uncover the intricate interplay among signals. The removal of this component will result in constructing a hypergraph that relies only on the attention mechanism. The attention mechanism further optimizes the PLV, and if it is removed, the hypergraph construction will be reverted to a method based on pristine synchronous analysis. In this context, MHSA-attention and MHSA-PLV denote distinct component exclusion modes. To delve deeper into the significance of these components, this study removed both components simultaneously and used the distance-based KNN algorithm to construct brain networks [25]. This approach helped identify the critical role of these components by eliminating potential confounding factors. Finally, the findings presented in Table IV intuitively demonstrate the indispensable functions of these two components in the MHSA framework.

F. Parameter sensitivity and analysis

The analysis focused on three key parameters that have a significant impact on the performance of MHSA: the dimension of the hidden layer (hidden), the learning rate (lr), and the regularization parameter (λ). Fig. 7 shows that the model achieves the best performance at hidden layer dimensions of 64 and 128. This result suggests that a higher-dimensional hidden layer is more suitable

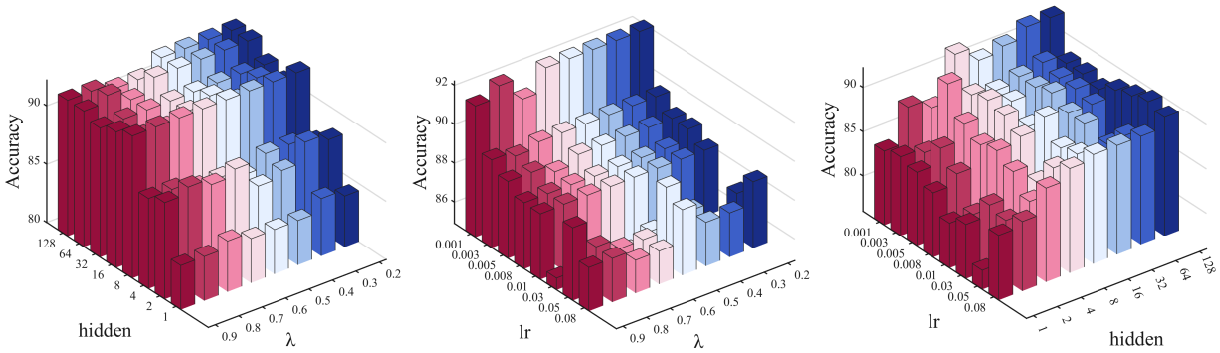

(a) lr = 0.001 (b) hidden = 64 (c) $\lambda = 0.2$

Fig. 7. Sensitivity of the three main hyperparameters in MHSA on NC vs. All TYPES of MCI detection task.

TABLE IV
CLASSIFICATION RESULTS BY 5-FOLD CROSS-VALIDATION WITH COMPETING METHODS.

Group	Method	Performance Metrics (%)			
		Accuracy	Sensitivity	Precision	F1
NC vs. EMCI	HGNN	76.02 ± 8.38	85.64 ± 9.94	81.02 ± 6.95	82.99 ± 7.03
	MHSA-PLV	75.09 ± 9.23	82.69 ± 11.54	82.62 ± 10.09	81.89 ± 6.98
	MHSA-attention	73.98 ± 3.55	79.74 ± 5.98	83.16 ± 6.99	80.96 ± 2.57
	MHSA	**86.96 ± 5.39**	**96.92 ± 3.77**	**86.61 ± 5.93**	**91.29 ± 3.29**
NC vs. MCI	HGNN	78.58 ± 11.47	88.36 ± 11.43	81.26 ± 9.74	84.11 ± 8.54
	MHSA-PLV	75.58 ± 15.18	74.36 ± 17.58	85.47 ± 11.05	78.98 ± 14.80
	MHSA-attention	73.08 ± 14.0	72.36 ± 17.39	82.97 ± 8.63	76.76 ± 13.95
	MHSA	**86.08 ± 9.98**	**98.0 ± 4.0**	**84.13 ± 10.42**	**90.26 ± 6.92**
NC vs. LMCI	HGNN	72.18 ± 15.87	72.00 ± 20.40	72.09 ± 21.07	70.52 ± 17.16
	MHSA-PLV	72.36 ± 21.37	64.0 ± 26.53	73.0 ± 28.21	67.44 ± 25.98
	MHSA-attention	77.82 ± 17.56	76.0 ± 19.60	78.0 ± 22.67	76.28 ± 19.29
	MHSA	**83.45 ± 15.56**	**84.0 ± 14.97**	**84.26 ± 20.40**	**83.13 ± 15.28**
NC vs. ALL MCI	HGNN	87.70 ± 3.81	**100.0 ± 0.0**	87.39 ± 3.62	93.23 ± 2.03
	MHSA-PLV	90.54 ± 5.13	**100.0 ± 0.0**	90.13 ± 5.0	94.74 ± 2.78
	MHSA-attention	87.19 ± 4.80	**100.0 ± 0.0**	86.99 ± 4.55	92.98 ± 2.57
	MHSA	**92.21 ± 3.66**	**100.0 ± 0.0**	**91.65 ± 3.68**	**95.60 ± 2.02**

for capturing features in brain networks than its lower-dimensional counterparts. Notably, our findings suggest that excessively high learning rates should be avoided to mitigate potential model performance degradation. In contrast, choosing larger values for the regularization parameter leads to satisfactory results. Regarding the remaining parameters common to deep learning models, a standardized analysis was conducted within a predefined range of values. This comprehensive parameter examination has provided profound insights into how changes in these parameters specifically affect model performance.

V. CONCLUSION

In this study, we proposed MHSA, a novel hypergraph modelling method via synchronous and attentive fusion for MCI detection. We are innovative in using PLV as a new method to analyze the phase synchronization of fMRI in the spectrum domain. Subsequently, we implemented a multi-scale feature fusion mechanism, and a temporal-spectrum fusion matrix was generated to fully reflect the continuous dynamic changes of brain regions. Furthermore, using the hypergraph and graph representation learning technology based on the derived matrix. Experiments verify that our approach manifests effectively in various types of MCI detection. In future work, we will explore the potential application of the MHSA model to other neurodegenerative diseases.

VI. ACKNOWLEDGMENT

This work was supported by the National Natural Science Foundation of China (Grants No.62106020, 62466042), the Inner Mongolia University High-level Talent Project (Grant No.10000-23112101), the Inner Mongolia Autonomous Region to Introduce High-Level Talent Research Support Project in 2023 (Grant No.13100-15112038), the Beijing Natural Science Foundation (Grant No.L211020), and the Science and Technology Program of the Joint Fund of Scientific Research for the Public Hospitals of Inner Mongolia Academy of Medical Sciences (Grant No.2023GLLH0004).

REFERENCES

[1] Y. Ding, C. Luo, C. Li, T. Lan, and Z. Qin, "High-order correlation detecting in features for diagnosis of alzheimer's disease and mild cognitive impairment," *Biomedical Signal Processing and Control*, vol. 53, p. 101564, 2019.

[2] W. Shao, Y. Peng, C. Zu, M. Wang, and D. Zhang, "Hypergraph based multi-task feature selection for multimodal classification of alzheimer's disease," *Computerized Medical Imaging and Graphics*, vol. 80, p. 101663, 2020.

[3] Y. Ji, Y. Zhang, H. Shi, Z. Jiao, S.-H. Wang, and C. Wang, "Constructing dynamic brain functional networks via hypergraph manifold regularization for mild cognitive impairment classification," *Frontiers in Neuroscience*, vol. 15, p. 669345, 2021.

[4] Q. Zuo, H. Wu, C. L. P. Chen, B. Lei, and S. Wang, "Prior-guided adversarial learning with hypergraph for predicting abnormal connections in alzheimer's disease," *IEEE Trans. Cybern.*, vol. 54, no. 6, pp. 3652–3665, 2024.

[5] Z. Xi, T. Liu, H. Shi, and Z. Jiao, "Hypergraph representation of multimodal brain networks for patients with end-stage renal disease associated with mild cognitive impairment," *Math. Biosci. Eng*, vol. 20, no. 2, pp. 1882–1902, 2023.

[6] W. Shao, Y. Peng, C. Zu, M. Wang, and D. Zhang, "Hypergraph based multi-task feature selection for multimodal classification of alzheimer's disease," *Comput. Medical Imaging Graph.*, vol. 80, p. 101663, 2020.

[7] D. Yao, J. Sui, M. Wang, E. Yang, Y. Jiaerken, N. Luo, P.-T. Yap, M. Liu, and D. Shen, "A mutual multi-scale triplet graph convolutional network for classification of brain disorders using functional or structural connectivity," *IEEE Transactions on Medical Imaging*, vol. 40, no. 4, pp. 1279–1289, 2021.

[8] J. Wang, H. Li, G. Qu, K. M. Cecil, J. R. Dillman, N. A. Parikh, and L. He, "Dynamic weighted hypergraph convolutional network for brain functional connectome analysis," *Medical Image Anal.*, vol. 87, p. 102828, 2023.

[9] Y. Ban, H. Lao, B. Li, W. Su, and X. Zhang, "Diagnosis of alzheimer's disease using hypergraph p-laplacian regularized multi-task feature learning," *J. Biomed. Informatics*, vol. 140, p. 104326, 2023.

[10] B. Mišić, Z. Fatima, M. K. Askren, M. Buschkuehl, N. Churchill, B. Cimprich, P. J. Deldin, S. Jaeggi, M. Jung, M. Korostil *et al.*, "The functional connectivity landscape of the human brain," *PLoS One*, vol. 9, no. 10, p. e111007, 2014.

[11] T. Lei, K. T. Bae, and T. P. Roberts, "A new methodology for phase-locking value: a measure of true dynamic functional connectivity," in *Medical Imaging 2012: Biomedical Applications in Molecular, Structural, and Functional Imaging*, vol. 8317, 2012, pp. 236–247.

[12] J. Xi, X.-L. Huang, X.-Y. Dang, B.-B. Ge, Y. Chen, and Y. Ge, "Classification for memory activities: Experiments and eeg analysis based on networks constructed via phase-locking value," *Computational and Mathematical Methods in Medicine*, vol. 2022, no. 1, p. 3878771, 2022.

[13] I. Alam, P. Lohariwal, D. Jalan, S. K. Saha, and A. Sinha, "Identifying extrinsic functional activation of brain regions using bold signals," in *2020 IEEE Region 10 Symposium (TENSYMP)*, 2020, pp. 222–225.

[14] M. Guirgis, Y. Chinvarun, M. Del Campo, P. L. Carlen, and B. L. Bardakjian, "Defining regions of interest using cross-frequency coupling in extratemporal lobe epilepsy patients," *Journal of neural engineering*, vol. 12, no. 2, p. 026011, 2015.

[15] Y. Ma, T. Zhang, Z. Wu, X. Mu, X. Liang, and L. Guo, "Multi-view brain networks construction for alzheimer's disease diagnosis," in *2023 IEEE International Conference on Bioinformatics and Biomedicine (BIBM)*, 2023, pp. 889–892.

[16] Y. Zhao, F. Zhou, B. Guo, and B. Liu, "Spatial temporal graph convolution with graph structure self-learning for early mci detection," in *2023 IEEE 20th International Symposium on Biomedical Imaging (ISBI)*, 2023, pp. 1–5.

[17] Y. Ma, W. Cui, J. Liu, Y. Guo, H. Chen, and Y. Li, "A multi-graph cross-attention-based region-aware feature fusion network using multi-template for brain disorder diagnosis," *IEEE Transactions on Medical Imaging*, vol. 43, no. 3, pp. 1045–1059, 2024.

[18] J. Liu, W. Cui, Y. Chen, Y. Ma, Q. Dong, R. Cai, Y. Li, and B. Hu, "Deep fusion of multi-template using spatio-temporal weighted multi-hypergraph convolutional networks for brain disease analysis," *IEEE Transactions on Medical Imaging*, vol. 43, no. 2, pp. 860–873, 2024.

[19] J. Wang, H. Li, G. Qu, K. M. Cecil, J. R. Dillman, N. A. Parikh, and L. He, "Dynamic weighted hypergraph convolutional network for brain functional connectome analysis," *Medical Image Anal.*, vol. 87, p. 102828, 2023.

[20] Y. Li, B. Yang, D. Pan, A. Zeng, L. Wu, and Y. Yang, "Early diagnosis of alzheimer's disease based on multimodal hypergraph attention network," in *2023 IEEE International Conference on Multimedia and Expo (ICME)*, 2023, pp. 192–197.

[21] Y. Wang, Y. Shi, Y. Cheng, Z. He, X. Wei, Z. Chen, and Y. Zhou, "A spatiotemporal graph attention network based on synchronization for epileptic seizure prediction," *IEEE J. Biomed. Health Informatics*, vol. 27, no. 2, pp. 900–911, 2023.

[22] Z.-M. Wang, R. Zhou, Y. He, and X.-M. Guo, "Functional integration and separation of brain network based on phase locking value during emotion processing," *IEEE Transactions on Cognitive and Developmental Systems*, vol. 15, no. 2, pp. 444–453, 2023.

[23] F. R. Kschischang, "The hilbert transform," *University of Toronto*, vol. 83, p. 277, 2006.

[24] P. Velickovic, G. Cucurull, A. Casanova, A. Romero, P. Liò, and Y. Bengio, "Graph attention networks," *CoRR*, vol. abs/1710.10903, 2017.

[25] Y. Feng, H. You, Z. Zhang, R. Ji, and Y. Gao, "Hypergraph neural networks," in *AAAI*, 2019, pp. 3558–3565.

[26] C. Cortes and V. Vapnik, "Support-vector networks," *Machine learning*, vol. 20, pp. 273–297, 1995.

[27] T. N. Kipf and M. Welling, "Semi-supervised classification with graph convolutional networks," in *ICLR (Poster)*, 2017.

[28] M. Chen, Z. Wei, Z. Huang, B. Ding, and Y. Li, "Simple and deep graph convolutional networks," in *ICML*, vol. 119, 2020, pp. 1725–1735.

[29] A. Cavallo, C. Grohnfeldt, M. Russo, G. Lovisotto, and L. Vassio, "GCNH: A simple method for representation learning on heterophilous graphs," in *IJCNN*, 2023, pp. 1–8.

[30] J. Chen, S. Chen, Z. Huang, J. Zhang, and J. Pu, "Exploiting neighbor effect: Conv-agnostic gnns framework for graphs with heterophily," *CoRR*, vol. abs/2203.11200, 2022.

[31] J. Huang, H. Shen, L. Hou, and X. Cheng, "Signed graph attention networks," in *ICANN (Workshop)*, vol. 11731, 2019, pp. 566–577.